Available online at www.sciencedirect.com
ScienceDirect
International Journal of Multiphase Flow 34 (2008) 260–271
International Journal of Multiphase Flow
www.elsevier.com/locate/ijmulflow

Accounting for finite-size effects in simulations of disperse particle-laden flows

S.V. Apte *, K. Mahesh, T. Lundgren

Department of Mechanical Engineering, Oregon State University, 204 Rogers Hall, Corvallis, OR 97331, United States
Department of Aerospace Engineering and Mechanics, University of Minnesota, 107, Akerman Hall, Minneapolis, MN 55455, United States

Received 27 November 2006; received in revised form 22 May 2007

Abstract

A numerical formulation for Eulerian–Lagrangian simulations of particle-laden flows in complex geometries is developed. The formulation accounts for the finite-size of the dispersed phase. Similar to the commonly used point-particle formulation, the dispersed particles are treated as point-sources, and the forces acting on the particles are modeled through drag and lift correlations. In addition to the inter-phase momentum exchange, the presence of particles affects the fluid phase continuity and momentum equations through the displaced fluid volume. Three flow configurations are considered in order to study the effect of finite particle size on the overall flowfield: (a) gravitational settling, (b) fluidization by a gaseous jet, and (c) fluidization by lift in a channel. The finite-size formulation is compared to point-particle representations, which do not account for the effect of finite-size. It is shown that the fluid displaced by the particles plays an important role in predicting the correct behavior of particle motion. The results suggest that the standard point-particle approach should be modified to account for finite particle size, in simulations of particle-laden flows.
Published by Elsevier Ltd.

Keywords: Particle-laden flows; LES/DNS; Point-particles; Particle–fluid interactions

1. Introduction

Many engineering problems involve two-phase flows, where particles of different shapes, sizes, and densities in the form of droplets, solid particles, or bubbles are dispersed in a continuum (gaseous or liquid) fluid. Numerical simulations of these flows commonly employ Lagrangian description for the dispersed phase and Eulerian formulation for the carrier phase. Depending on the volumetric loading of the dispersed phase two regimes can be identified: dilute ($d_p \ll l$) and dense ($d_p \approx l$), where d_p is the particle diameter, and l the inter-particle distance (Elghobashi, 1984). Furthermore, the grid resolution (Δ) used for solution of the carrier phase could be such that the particles are *subgrid* ($d_p \ll \Delta$), *partially resolved* ($\Delta \sim d_p$), or *fully resolved* ($\Delta \ll d_p$). Different numerical approaches are necessary to simulate the various regimes of the flow. Typical applications (e.g. spray combustion, liquid atomization, fluidized bed combustion, aerosol transport, and bubbly flows) involve millions of dispersed particles in a turbulent flow where the particle diameter could be smaller than, or comparable to the Kolmogorov length scale. To simulate these flows using fully resolved direct numerical simulation (where the forces acting on a particle are computed and not modeled) requires enormous computational resources, and the use of such methods are commonly restricted to small number of particles (≈1000, Kajishima and Takiguchi, 2002; Choi and Joesph, 2001).

To facilitate simulations of large number of dispersed particles in complex turbulent flows the 'point-particle' (PP) assumption is commonly invoked. The particle size is assumed to be smaller than the grid size and the forces exerted by the particles onto the fluid are represented as point-sources at the position of the centroid of the

* Corresponding author. Tel.: +1 541 737 7335; fax: +1 541 737 2600.
E-mail address: sva@engr.orst.edu (S.V. Apte).

0301-9322/$ - see front matter Published by Elsevier Ltd.
doi:10.1016/j.ijmultiphaseflow.2007.10.005

particle. Typically, direct numerical simulation (DNS), large-eddy simulation (LES) or Reynolds-averaged Navier Stokes (RANS) equations are used for the carrier phase, whereas the motion of the dispersed phase is modeled through drag and lift laws (Crowe et al., 1998). Several simulations of particle-laden flows have been performed with the carrier fluid simulated using DNS (Reade and Collins, 2000; Rouson and Eaton, 2001; Xu et al., 2002), LES (Wang and Squires, 1996; Apte et al., 2003a,b; Segura et al., 2004; Moin and Apte, 2006), and RANS (Sommerfeld et al., 1992), where the dispersed phase is assumed to be subgrid (so $d_p < L_K$, the Kolmogorov length scale, for DNS, whereas $d_p < \Delta$, the grid size, in LES or RANS).

Recently, Apte et al. (2003a, 2004) used LES for the carrier phase along with point-particle assumption for swirling, separated flows in coaxial combustors and obtained good agreement with the available experimental data. The particle dispersion characteristics and residence times were accurately predicted using an unstructured grid LES solver (Mahesh et al., 2004). However, modeling the dispersed phase using the point-particle approach does not always yield accurate results. For moderate loadings and wall-bounded flows, Segura et al. (2004) have shown that the point-particle approximation fails to predict turbulence modulation in agreement with experimental values. In order to capture the same level of turbulence modulation observed in experiments, it was required to artificially increase the particle loadings by an order of magnitude when using the point-particle approach. In addition, if the particle size is comparable to the Kolmogorov scale (for DNS) or the grid size (for LES/RANS), simple drag/lift laws typically employed in point-particle approach do not capture the important features of unsteady wake effects commonly observed in full resolved DNS studies (Burton and Eaton, 2003; Bagchi and Balachandar, 2003). These effects become even more pronounced in dense particulate regions. Also, the effect of wake behind a particle and its rotation become important when the particle diameters are large. In addition, in many practical applications, the local particle size and concentrations may vary substantially. For example, in liquid fuel atomization process in propulsion systems, the droplet sizes may range from 1 mm to 1 μm with dense regions near the injector nozzle. The point-particle assumption is invalid under these conditions, but still is widely used in simulations of multiphase flows (Apte et al., 2003b, 2004; Moin and Apte, 2006). The particle volume fractions are *often* neglected in these simulations owing to the increased complexity of the governing equations as well as numerical stiffness they impose in the dense particle regions. The wake effects and particle rotation are also neglected in these simulations. In the present paper, emphasis is placed on improving the point-particle assumption by accounting for their finite-size. Further modifications to account for wake effects and particle rotation are possible; but are deferred to future work.

We attempt to extend the point-particle approximation by accounting for the volumetric effects of the particles and the corresponding volume displacement in the carrier phase. Only isothermal, incompressible flows are considered; however, the methodology can be readily extended to variable density and reacting flows. In this finite-size particle approach (FSP), the particles are still assumed to be subgrid, and the forces acting on them are modeled using modified drag and lift laws. The finite-size of the particle is accounted by modifying the carrier phase continuity and momentum equations to include the fluid volume fraction (Θ_f). The effect of the particles onto the carrier fluid is felt through a source term in the momentum equations similar to the two-way coupling of point-particles. In addition, the fluid volume displaced by the particles also affect the continuity and momentum equations. Here we attempt to show that these effects of volumetric displacement of the carrier fluid can capture some of the important effects observed in fully resolved DNS studies of particle-laden flows. The effects are pronounced in regions where particles are clustered together.

The formulation was originally put forth by Dukowicz (1980) in the context of spray simulations and later modified by Joseph and Lundgren (1990) based on mixture theory. Andrews and O'Rourke (1996) developed a multiphase particle-in-cell (PIC) algorithm on structured grids based on the Eulerian–Lagrangian formulation for dense particulate flows. A similar formulation has recently been applied to bubbly flows at low bubble concentrations (up to 0.02) to investigate the effect of bubbles on drag reduction in turbulent flows (Xu et al., 2002; Ferrante and Elghobashi, 2004). Several studies on laminar dense granular flows (Patankar and Joseph, 2001a; Snider, 2001) also use this approach. However, none of these studies identify the effects of the fluid displacement by the dispersed phase as compared to the standard point-particles. In this work, the numerical framework for multiphase flows developed in Apte et al. (2003a,b, 2004) is extended to account for the dispersed phase volume fraction, and inter-particle collisions. The finite-size and point-particle approaches are compared, and the effect of fluid volume displacement by the dispersed phase is elucidated through numerical examples. We investigate three model problems for dense rigid particulate flows: (a) gravitational settling, (b) fluidization by a gaseous jet, and (c) fluidization by lift in a channel flow. The first two problems also serve as validation cases for the finite-size approach where comparisons with prior analytical and numerical studies are made. The particle-laden channel flow illustrates that the finite-size effects become important in the near-wall regions and should be accounted for in Eulerian–Lagrangian simulations.

The paper is organized as follows. Section (2) describes mathematical formulation of the governing equations. The numerical method is then outlined in Section (3), where gravitational settling (4.1), gas–solid fluidization (4.2), and fluidization by lift (4.3) are considered. A brief summary in Section (5) concludes the paper.

2. Mathematical formulation

The formulation consists of the Eulerian fluid and Lagrangian particle equations, and accounts for the displacement of the fluid by the particles, as well as the momentum exchange between the two phases (Joseph and Lundgren, 1990).

2.1. Gas-phase equations

The fluid mass per unit volume satisfies the continuity equation

$$\frac{\partial}{\partial t}(\rho_f \Theta_f) + \nabla \cdot (\rho_f \Theta_f \mathbf{u}_f) = 0, \tag{1}$$

where ρ_f, Θ_f, and $\mathbf{u}_f$ are fluid density, volume fraction, and velocity, respectively. The divergence operator in the continuity equation can be expanded to show that

$$\nabla \cdot \mathbf{u}_f = -\frac{1}{\Theta_f}\left(\frac{\partial \Theta_f}{\partial t} + \mathbf{u}_f \cdot \nabla \Theta_f\right), \tag{2}$$

i.e., the average velocity field of the fluid phase does not satisfy a 'divergence-free' condition even if we consider an incompressible suspending fluid. The particle volume fraction, $\Theta_p = 1 - \Theta_f$ is defined as

$$\Theta_p(\mathbf{x}_{\mathrm{cv}}) = \sum_{p=1}^{N_p} V_p \mathscr{G}_\sigma(\mathbf{x}_{\mathrm{cv}}, \mathbf{x}_p), \tag{3}$$

where the summation is over all particles N_p that will influence the computation cell (cv), with volume (V_{cv}) and centroid at $\mathbf{x}_{\mathrm{cv}}$. Here $\mathbf{x}_p$ is the particle location, and V_p the volume of a particle. Particles will be assumed spherical, however, non-spherical particles can also be modeled by using an effective diameter and modified drag laws (Crowe et al., 1998). The interpolation function, $\mathscr{G}_\sigma$, effectively transfers a Lagrangian quantity to give an Eulerian field (*per unit volume*, V_{cv}, of the grid cell containing the particle centroid) on the underlying grid and is defined later. The fluid momentum equation is (Joseph and Lundgren, 1990)

$$\frac{\partial}{\partial t}(\rho_f \Theta_f \mathbf{u}_f) + \nabla \cdot (\rho_f \Theta_f \mathbf{u}_f \mathbf{u}_f) = -\nabla(\Theta_f p) + \nabla \cdot (\mu_f \mathbf{D}_c) + \mathbf{F}, \tag{4}$$

where p is the dynamic pressure, μ_f is the viscosity of the fluid, and $\mathbf{D}_c = \nabla \mathbf{u}_c + \nabla \mathbf{u}_c^{\mathrm{T}}$ is the average deformation-rate of the fluid–particle composite, $\mathbf{u}_c = \Theta_f \mathbf{u}_f + \Theta_p \mathbf{u}_s$ is the composite velocity of the mixture, and $\mathbf{F}$ is the force per unit volume that the particles exert on carrier fluid. These equations are derived in detail for constant density flows in Joseph and Lundgren (1990). Here, $\mathbf{u}_s$ is the average particle velocity given as

$$\Theta_p \mathbf{u}_s = \sum_{p=1}^{N_p} V_p \mathscr{G}_\sigma(\mathbf{x}_{\mathrm{cv}}, \mathbf{x}_p)\mathbf{u}_p, \tag{5}$$

where $\mathbf{u}_p$ is the particle velocity.

2.2. Particle-phase equations

The positions and velocities of individual particles are obtained by solving the following ordinary differential equations for each particle p:

$$\frac{\mathrm{d}}{\mathrm{d}t}(\mathbf{x}_p) = \mathbf{u}_p, \tag{6}$$

$$m_p \frac{\mathrm{d}}{\mathrm{d}t}(\mathbf{u}_p) = \mathbf{F}_p, \tag{7}$$

where $\mathbf{x}_p$ is the particle position, $\mathbf{u}_p$ is the particle velocity, m_p the particle mass, $\mathbf{F}_p = m_p \mathbf{A}_p$ is the total force acting on the particle, and $\mathbf{A}_p$ is the particle acceleration given in Eq. (8).

The forces on a particle may consist of the standard hydrodynamic drag force, dynamic pressure gradient, gradient of viscous stress in the fluid phase, history force, inter-particle collision, and buoyancy force and are well described by the Basset–Boussinesq–Oseen (BBO) equations (Crowe et al., 1998). In the present work, we assume that the particle forces consist of drag, collision and gravitational acceleration only, and neglect all other terms. For high density ratios ($\rho_p/\rho_f \sim 1000$), these assumptions are generally considered valid (Apte et al., 2003a). We emphasize the effect of variations in particle volume fraction on the overall flowfield and particle motion.

The particle acceleration $\mathbf{A}_p$ is defined as

$$\mathbf{A}_p = D_p(\mathbf{u}_{f,p} - \mathbf{u}_p) + \left(1 - \frac{\rho_f}{\rho_p}\right)\mathbf{g} + \mathbf{A}_{cp}, \tag{8}$$

where $\mathbf{A}_{cp}$ is the acceleration due to inter-particle forces, and $\mathbf{u}_{f,p}$ is the fluid velocity at the particle location. The inter-particle force is modeled by the discrete-element method of Cundall and Strack (1979). The inter-particle repulsive force F_{pj}^{P-P} on parcel p due to collision with parcel j is given by

$$F_{pj}^{P-P} = \begin{cases} 0 & \text{for } d_{pj} \geqslant (R_{p,p} + R_{p,j} + \alpha), \\ \left(k_c \delta_{pj}^{3/2} - \eta_c(\mathbf{u}_p - \mathbf{u}_j)\cdot \mathbf{n}_{pj}\right)\mathbf{n}_{pj} & \text{for } d_{pj} < (R_{p,p} + R_{p,j} + \alpha), \end{cases} \tag{9}$$

$$\delta_{pj} = (R_{p,p} + R_{p,j} + \alpha) - d_{pj}, \tag{10}$$

$$\mathbf{F}_{jp}^{P-P} = -\mathbf{F}_{pj}^{P-P}, \tag{11}$$

where d_{pj} is the distance between the center of the pth and jth parcels, $\mathbf{n}_{pj}$ is the unit vector from the center of parcel j to that of parcel p, α is the force range, k_c the stiffness parameter, and η_c the damping parameter, and $R_p = (3V_p/4\pi)^{1/3}$ is the radius of each particle in a given parcel. Patankar and Joseph (2001b) used the following expressions to compute the damping parameter:

$$\eta_c = 2\alpha\sqrt{\frac{m_p k_c}{1+\alpha^2}},$$

$$\alpha = -\ln(e/\pi),$$

where e is the coefficient of restitution and $m_p = N_p \rho_p V_p$ is the parcel mass. Similarly, the parcel-wall force ($\mathbf{F}_{pw}^{P-W}$) on parcel p due to collision with wall w is

$$\mathbf{F}_{pw}^{P-W} = \begin{cases} 0 & \text{for } d_{pw} \geqslant (R_{p,p} + \alpha), \\ \left(k_c \delta_{pw}^{3/2} - \eta_c(\mathbf{u}_p) \cdot \mathbf{n}_{pw}\right)\mathbf{n}_{pw} & \text{for } d_{pw} < (R_{p,p} + \alpha), \end{cases} \tag{12}$$

$$\delta_{pw} = (R_{p,p} + 2\alpha) - d_{pw}, \tag{13}$$

where d_{pw} is the distance between the center of the parcel p and the wall w, and $\mathbf{n}_{pw}$ is the unit vector from the wall to the center of the parcel. The total collision force is obtained by looping over all particles and walls. The corresponding particle acceleration is obtained by dividing the collision force by the parcel mass.

The drag force is caused by the motion of a particle through the gas. D_p is defined as

$$D_p = \frac{3}{8} C_d \frac{\rho_f}{\rho_p} \frac{|\mathbf{u}_{f,p} - \mathbf{u}_p|}{R_p}. \tag{14}$$

It should be noted that the above formulation for drag forces and the inter-particle collisions are similar that used in point-particle approaches, however, may not be adequate for finite-size particles. Models for other forces such as lift force, history force as well as modifications to the collision and drag forces may become necessary. However, the focus of the current paper is to show that, even without improved models for the above forces, the finite-size approach can capture some of the basic flow features in particle-laden flows which cannot be captured by the point-particle approach. Here, C_d is the drag coefficient and is given by (Gidaspow, 1994)

$$C_d = \frac{24}{Re_p}(1 + aRe_p^b)\Theta_f^{-2.65}, \quad \text{for } Re_p < 1000 \tag{15}$$

$$= 0.44\Theta_f^{-1.8}, \quad \text{for } Re_p \geqslant 1000, \tag{16}$$

where $R_p = (3V_p/4\pi)^{1/3}$ is the particle radius, $Re_p = 2\rho_f \Theta_f |\mathbf{u}_{f,p} - \mathbf{u}_p| R_p/\mu_f$ is the particle Reynolds number, $a = 0.5$ and $b = 0.687$. There is an indirect collective effect in this drag term; when there is a dense collection of particles passing through the fluid, the inter-phase momentum exchange term in Eq. (4) will cause $\mathbf{u}_f$ to approach the particle velocity, $\mathbf{u}_p$, thus decreasing the drag on a particle, a *drafting* effect. The inter-phase momentum transfer function per unit volume in Eq. (4) is given as

$$\mathbf{F}(\mathbf{x}_{cv}) = \sum_{p=1}^{N_p} \mathscr{G}_\sigma m_p D_p (\mathbf{u}_{f,p} - \mathbf{u}_p). \tag{17}$$

3. Numerical method

In this work, the numerical scheme for unstructured, arbitrary shaped elements developed by Mahesh et al. (2004) is modified to account for the fluid volume fraction. The changes in local fluid volume fractions requires solution of a *variable density* flowfield as opposed to the constant density, incompressible flows studied in Apte et al. (2003a,b) and Mahesh et al. (2004). The other important feature of this work is use of a Gaussian interpolation operator from the Lagrangian points to the Eulerian grid. Prior studies on dense granular flows by Patankar and Joseph (2001a) and Snider (2001) used bilinear interpolation functions to interpolate Lagrangian fields onto the Eulerian grid nodes. The interpolation stencil utilized 26 neighboring grid cells in three-dimensions. We generalize these interpolations to unstructured, arbitrarily shaped elements, using a Gaussian function centered at the particle centroid for interpolation. This function is given by

$$\mathscr{G}_\sigma(\mathbf{x}, \mathbf{x}_p) = \frac{1}{\left(\sigma\sqrt{2\pi}\right)^3} \exp\left[-\frac{\sum_{k=1}^{3}(x_k - x_{p,k})^2}{2\sigma^2}\right]. \tag{18}$$

Here we assume that $V_p < V_{cv}$, and use uniform grid cells in all computations, with $\sigma = V_{cv}^{1/3}$. Accordingly, σ remains the same throughout the computations. The interpolation operator is applied to all the neighbors of this cv (having at least one grid node in common). Similar interpolation has been used in the context of fully resolved simulations of particles (Maxey and Patel, 2001a). Further investigation of the choice and effect of σ on non-uniform meshes is necessary and is beyond the scope of this paper.

The advantage of using a Gaussian-based interpolation kernel is that it can be readily used to transfer particle quantities to an Eulerian field on arbitrary shaped unstructured grids. Consistent interpolations preserving higher-order moments can be derived based on Gaussian-kernels and are useful for conservative properties of particle-in-cell methods (Eldredge et al., 2002). Although Gaussian kernels provide smooth interpolations they do not have a compact support. This interpolation scheme has been proven very effective in large-eddy simulations of *point-particle* laden turbulent flows in coaxial combustors on unstructured grids (Apte et al., 2003a). In addition, $\mathscr{G}$ is normalized to satisfy

$$\int_{V_{cv}} \mathscr{G}_\sigma(\mathbf{x}_{cv}, \mathbf{x}_p) \mathrm{d}V = 1, \tag{19}$$

where the integration is performed over the cv containing the particle and all of its neighbors. The final step is necessary to enforce mass (or volume) conservation. The resulting Θ_p will be smooth and mass-conserving as the particles move from one computational cell to another. The steps in solving the coupled fluid–particle equations are given below. We use a semi-implicit scheme for the fluid solver, however, the inter-phase momentum exchange terms are treated explicitly.

- *Step 1:* Advance the particle positions and velocities using a third-order Runge–Kutta scheme. We compute the collision force at each Runge–Kutta iteration. Com-

pute the volume fraction field at the new particle locations and set the density $\rho = \rho_f \Theta_f$.

- *Step 2:* Advance the fluid momentum equations (from t^n to t^{n+1}) using the fractional step algorithm, with the inter-phase force, **F**, treated explicitly. As in all fractional step schemes, this advancement is done in two steps. First an intermediate velocity field u_i^* is obtained at the control volume centers. This velocity field may not satisfy the continuity equation and hence is an approximation to the actual velocity field at time level t^{n+1}

$$\frac{\rho^{n+1}\hat{u}_i - \rho^n u_i^n}{\Delta t} + \frac{1}{2V_{\text{cv}}}\sum_{\text{faces of cv}}\left[u_{i,f}^n + \hat{u}_{i,f}\right] g_N^{n+1/2} A_f = \frac{1}{2V_{\text{cv}}}\sum_{\text{faces of cv}} \mu_f \left(\frac{\partial \hat{u}_{i,f}}{\partial x_j} + \frac{\partial u_{i,f}^n}{\partial x_j}\right) A_f + F_i^n, \tag{20}$$

where f represents the face values, N the face-normal component, $g_N = \rho u_N$, and A_f is the face area. The velocity components at the faces ($u_{i,f}$) are obtained by taking the arithmetic average of velocities at two adjacent control volumes having a common face.

- *Step 3:* Interpolate the velocity fields to the faces of the control volumes and consider the corrector step:

$$\frac{\rho^{n+1}u_i^{n+1} - \rho^{n+1}\hat{u}_i}{\Delta t} = -\frac{\delta p}{\delta x_i}, \tag{21}$$

$$\frac{\rho_f^{n+1}u_N^{n+1} - \rho_f^{n+1}\hat{u}_N}{\Delta t} = -\frac{\delta p}{\delta x_N}, \tag{22}$$

where $\hat{u}_N = \hat{u}_{i,f} n_{i,f}$ is the approximation for face-normal velocity and $n_{i,f}$ are the components of the face-normal. The face-based density ρ_f is obtained by arithmetic average of the adjacent control volume-based densities. The face-normal pressure gradient $\frac{\delta p}{\delta x_N}$ and the gradient in pressure at the cv-centroids are related by the area-weighted least-squares interpolation developed by Mahesh et al. (2004).

- *Step 4:* The Poisson equation for pressure is obtained by taking the divergence of the face-normal velocity component in Step 3 to obtain

$$\frac{1}{V_{\text{cv}}}\sum_{\text{faces of cv}} \frac{\delta p}{\delta x_N} A_f \Delta t = \frac{1}{V_{\text{cv}}}\sum_{\text{faces of cv}} \rho_f^{n+1}\hat{u}_{i,f} A_f + \frac{\delta \rho}{\delta t}. \tag{23}$$

Here we have made use of the continuity equation

$$\frac{\delta \rho}{\delta t} = -\frac{1}{V_{\text{cv}}}\sum_{\text{faces of cv}} \rho_f^{n+1} u_{i,f}^{n+1} A_f. \tag{24}$$

- *Step 5:* Reconstruct the pressure gradient, compute new face-based velocities, and update the cv-velocities using the least-squares interpolation used by Mahesh et al. (2004).

Note that, in the above formulation if we set $\Theta_f = 1$ in all computational cells, we obtain $\rho = \rho_f$, and $\frac{\partial \rho}{\partial t} = 0$. This results in the standard incompressible flow equations used for the point-particle approach.

4. Results

In order to reduce the number of particles tracked in the following simulations, the concept of 'parcels' is used. A parcel consists of a collection of particles having same properties, e.g. the diameter. The parcel is identified by the number of particles it consists, the diameter of each particle, the position and velocity of the centroid of the particles. The parcel approach has been used in spray simulations (Apte et al., 2003b; Moin and Apte, 2006). Note that the present formulation can be applied directly to track each particle, however, would require increased computational time.

4.1. Gravitational settling

We first simulate sedimentation of solid particles under gravity in a rectangular box. Details of the simulation are given in Table 1. Initial parcel positions are generated randomly over the entire length of the box. These parcels are then allowed to settle through the gas-medium under gravity. The dominant forces on the particles include gravity and inter-particle/particle–wall collision. As the particles hit the bottom wall of the box, they bounce back and stop the incoming layer of particles, and finally settle to a close-pack limit ($\Theta_p \sim 0.6$). Fig. 1a shows the time evolution of particle positions in the rectangular box starting with an initial random distribution for finite-size particles. The particles eventually settle down with close-packing near the bottom wall. As the particles settle, they accelerate the fluid flow upwards, which in turn slows the rate of particle settling.

The simulation was also performed using the point-particle approach by neglecting the particle volume fraction (by setting $\Theta_f = 1$). The collision between the particles and with the wall are simulated using the same collision model. Note that the point-particle formulation *does not* include any displacement of the carrier fluid due to particle motion. Fig. 1b shows the temporal evolution of the interface location between the particles and the surrounding fluid obtained using finite-size point-particle formulations. Both approaches predict similar interface evolution which is well approximated by the analytical estimate $h = gt^2/2$. This is because the dominant forces acting on the particles are gravity and inter-particle collision. In the finite-size approach, as the particles settle, they accelerate the fluid,

Table 1
Parameter description for gravity-dominated sedimentation

Computational domain	$0.2 \times 0.6 \times 0.0275$ m
Grid	$10 \times 30 \times 5$
Fluid density	1.254 kg/m^3
Particle density	2500 kg/m^3
Number of parcels	1000
Particles per parcel	3375
Diameter of particles	500 μm
Initial particle concentration	0.2

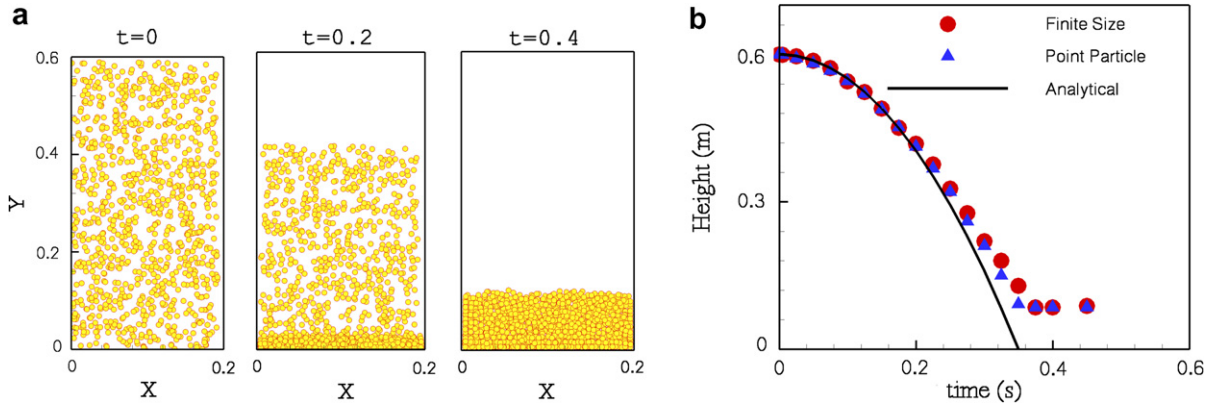

Fig. 1. Gravity-dominated sedimentation: (a) temporal evolution of particle distribution, and (b) comparison of height from the bottom wall using point and finite-size particles to the analytical solution ($H = H_0 - 0.5gt^2$).

however, the effect of the drag force and also the fluid displaced by the particle motion is found negligible. Small differences in the interface evolution are observed between the finite-size and point-particle formulations at later stages when the variations in local fluid volume displacements become comparable to the gravity and collision forces.

4.2. Gas–solid fluidization

We consider the problem of fluidization of solid particles arranged in an array at the bottom of a rectangular box. Fluidization is achieved by a jet of gas issuing from the bottom of the box. The flow parameters are outlined in Table 2. Here, the particle motion is mostly dominated by the hydrodynamic drag force and the collision model is important close to the wall, and near the close-pack limit.

Fig. 2a shows the position of parcels at different times during bubbling fluidization obtained using the finite-size formulation. Parcel diameters are drawn to scale. The jet issues from the bottom wall, pushes the particles away from the central region, and creates a gas-bubble in the center. The particles collide with each other and the wall, and are pushed back towards the central jet along the bottom wall. They are then entrained by the jet and levitated. This eventually divides the central bubble into two. At future times (not shown), the particles tend to move upward and collide with the upper wall and remain levitated. The computational results are in good agreement with the simulations of Patankar and Joseph (2001a). Similar results have been reported using Eulerian–Eulerian approach in two-dimensions by Ding and Gidaspow (1990) and Gidaspow (1994).

Table 2
Parameter description for the simulation of fluidization by a gas jet

Computational domain	$0.2 \times 0.6 \times 0.0275$ m
Grid	$10 \times 30 \times 5$
Gas jet velocity	9 m/s
Jet diameter	0.04 m
Fluid density	1.254 kg/m^3
Particle density	2500 kg/m^3
Number of parcels	2880
Particles per parcel	3375
Diameter of particle	500 μm
Initial particle concentration	0.4

Fig. 2b shows the corresponding temporal evolution of particles predicted by the point-particle approach using the same collision model as above. With point-particles, the only interaction between the two phases is through the momentum transfer terms. Fig. 2b clearly demonstrates that this term alone does not represent the inter-phase interactions properly. With the finite-size formulation, the particles affect the fluid flow in two ways: (i) the inter-phase interaction force and (ii) the displacement of fluid through particle motions. Note that the volumetric displacements are modeled through the fluid volume fraction (Θ_f) which modifies the momentum and continuity equations. In addition, it also alters the drag law through Eq. (15).

In order to investigate the effect of the drag law, we repeated the simulation using the finite-size formulation, however, by setting ($\Theta_f = 1$) only in Eq. (15). This corresponds to using the same drag law as for point-particle approach. The effect on the overall particle distribution was negligible.

The differences in particle evolutions predicted by point-particle and finite-size approaches thus can be attributed to the direct effect of variations in particle volume fraction fractions. Fig. 3a and b shows the corresponding evolution of the velocity vectors in the symmetry section obtained from finite-size and point-particle formulations, respectively. Every other point is plotted for clarity of the vector plot. The differences in flow patterns near the bottom wall are clearly visible. With the point-particle approach, a recirculation zone is observed around the jet location. The flowfield is typical of a jet entering a sudden expansion. The velocity of the jet is modulated because of the drag force exerted by the presence of particles. This recirculation region is absent when using the finite-size formulation. The entire flowfield near the bottom wall indicates diverging trajectories away from the jet. This flowfield thus pushes

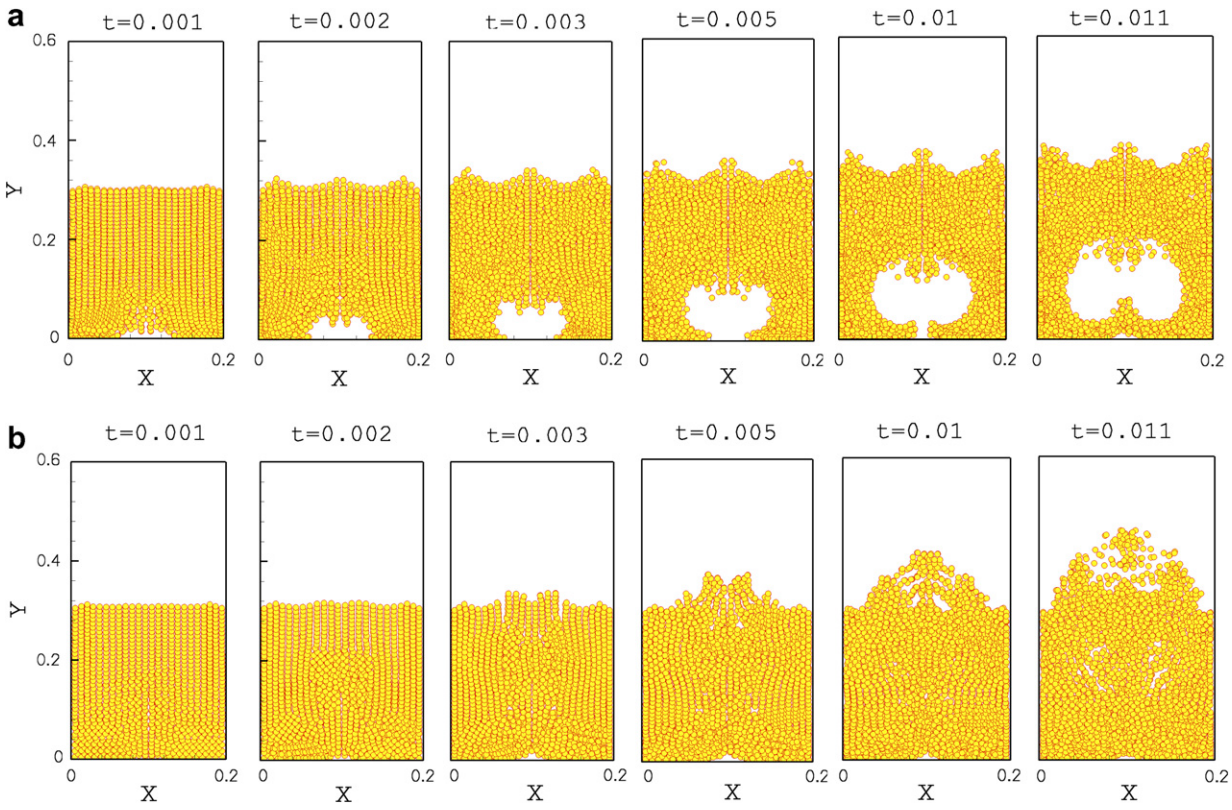

Fig. 2. Temporal evolution of particle distribution during fluidization by a gas jet from the bottom wall: (a) finite-size particles; (b) point-particles.

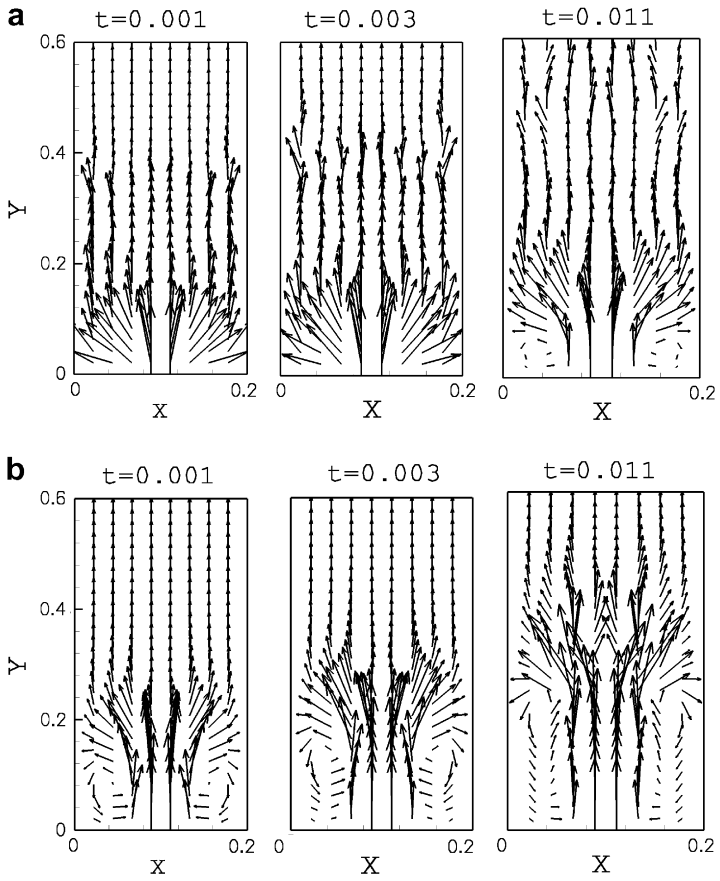

Fig. 3. Temporal evolution of the gas-phase velocity vectors in fluidization by jet: (a) finite-size particles; (b) point-particles.

the particles toward the walls creating a void near the jet origin (see Fig. 2a). The particles are clustered together into close-pack near the side walls and slow down the fluid flow. The gravitational force then moves the particles toward the jet center at later times ($t = 0.011$ s). The fluid then shows the presence of small recirculation zone around the jet (Fig. 3a, $t = 0.011$ s). On the contrary, the corresponding velocity field for the point-particle approach shows upward propagation of the jet, and recirculation zones.

Fig. 4a and b shows the normalized axial pressure gradient and kinetic energy along the axis of the jet at different times. The pressure gradient and kinetic energy distribution obtained from the finite-size and point-particle approaches are drastically different. The finite-size approach shows large variations in the axial pressure gradient. As the jet enters the rectangular chamber, it encounters a mass of densely packed particles initially at rest. The inertia of the particles decelerates the jet, and creates an axial pressure gradient similar to flow over a bluff body. In the present case, the particles are pushed away by the jet, which in turn decreases the kinetic energy along the jet centerline. The formation and growth of a gas-bubble trapped by the particles pushes the bed upward. With the point-particle formulation, the kinetic energy of the fluid close to the jet opening remains mostly constant, and then decreases further away from the bottom wall. This shows that the representation of the inter-phase momentum exchange as point-sources cannot correctly capture the blocking effects created by particle clusters.

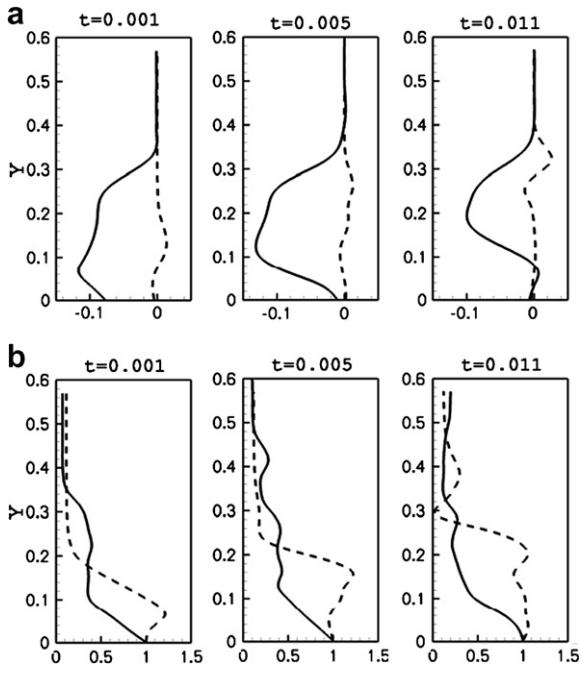

Fig. 4. Temporal evolution of depth-averaged (a) normalized axial pressure gradient (centerline $(\frac{\partial p}{\partial x})/\rho_{\text{jet}} U_{\text{jet}}^2$) and (b) normalized kinetic energy along the centerline of the jet (centerline $\frac{\text{KE}}{\text{KE}_{\text{jet}}}$) – solid line: finite-size particles, dashed line: point-particles.

In order to evaluate the effect of number of parcels on the temporal evolution of the parcels, and the gas-bubble patterns seen in Fig. 2a, we repeated the calculation using fewer parcels. Fig. 5 shows compares results obtained, using 2880 and 720 parcels. With reduced number of parcels, we keep the number of particles associated with each parcel the same, to maintain the same mass-loading of the particulate phase. The central bubble pattern is visible, even with small number of parcels. This verifies that the inter-parcel collision model as well as the variation of the particle volume fraction Θ_p is well captured by our Gaussian kernel-based interpolation scheme.

4.3. Fluidization by lift of spherical particles

The transport of particles by fluids in coal–water slurries, hydraulically fractured rocks in oil-bearing reservoirs, bed-load transport in rivers and canals and their overall effect on the river bed erosion, are important scientific and industrial issues in particulate flows. In order to understand fluidization/sedimentation in such conduits, Choi

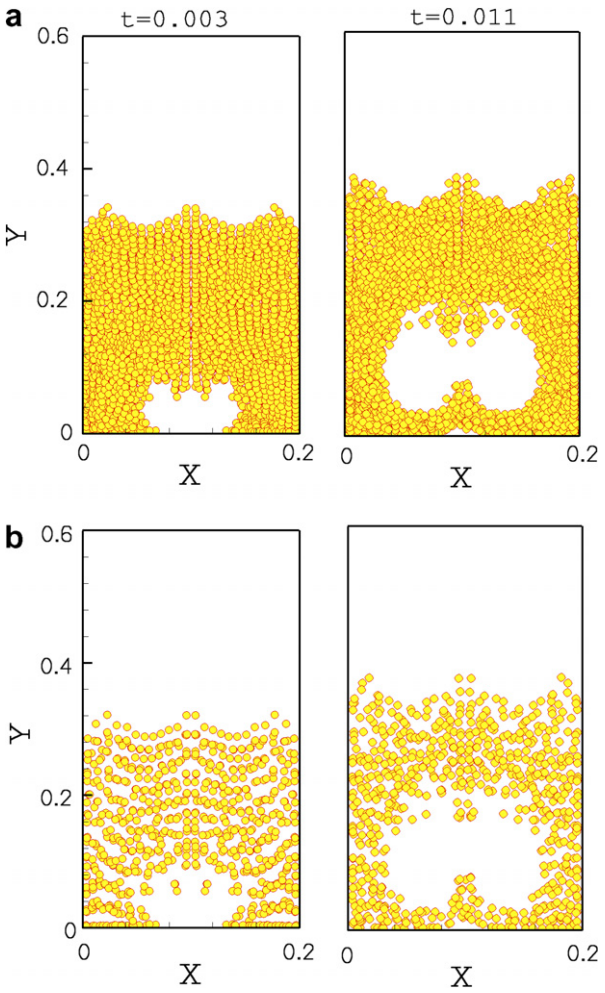

Fig. 5. Effect of number of parcels on the time evolution during fluidization by a gas jet from the bottom wall: (a, c) 2880, (b, d) 720 parcels.

and Joesph (2001) performed a fully resolved two-dimensional DNS study of flow over circular cylinders (300 particles) arranged at the bottom of a channel in plane Poisuille flow. The forces on particles were computed numerically and not modeled. They observed that with sufficient pressure gradient across the channel, the particles initially at rest in the lower half of the channel start moving and roll over the wall. The particle rotation in a shear flow generates lift and the channel is fluidized after some time.

The parameters used for this simulation are given in Table 3. As opposed to (Choi and Joesph, 2001), our simulations are three-dimensional with circular spheres arranged at the bottom of the channel, and the particle densities are 10 times higher ($\rho_p/\rho_f \approx 10$). These higher densities were chosen to ensure significant effects of the interphase momentum exchange. Fig. 6 shows the temporal evolution of particle positions and contours of volume fraction field on the left, and fluid axial velocity on the right. The two-way coupling between the particle and fluid momentum equations, decelerates the fluid in the bottom half of the channel, and the particles accelerate from rest. The particles in the upper layers move faster than those close to the wall. As the particles move from one grid cell to another, they push fluid out due to the gradients in volume fraction in the continuity equation. The volume displacement due to particles sets up instability waves, as seen from the axial velocity and volume fraction contours imparting vertical velocity to the particles. The simulation of this case with point-particle approach does not produce any lift of the particles, and the particles continue to move in laminar layers.

Table 3
Parameter description for the simulation of fluidization of spherical particles in a Poisuille flow

Computational domain	$63 \times 12 \times 12$ cm
Grid	$20 \times 11 \times 10$
Fluid density	1 g/cm^3
Fluid viscosity	1 P
Particle density	10 g/cm^3
Diameter of particles	0.9 cm
Number of particles	3780
Array height (from bottom wall)	4.75 cm
Initial centerline velocity	360 cm/s
Pressure gradient	20 dyne/cm^3

In order to further understand the effect of the finite-size approach, we plot the mean axial velocity variations in the vertical direction at $t = 0$ and $t = 0.2$ s in Fig. 7a. The mean velocity is obtained by averaging in the axial and spanwise (homogeneous) directions. Also plotted are the corre-

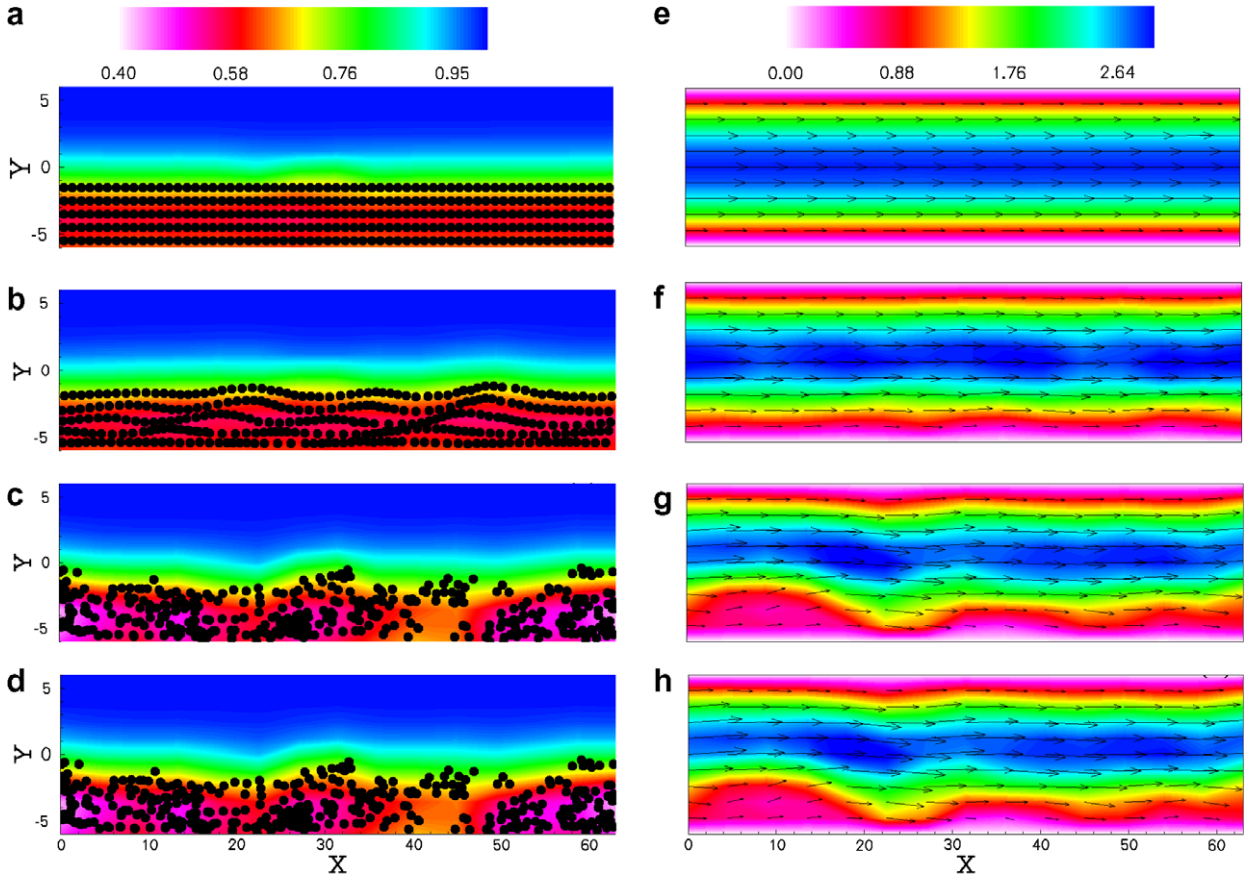

Fig. 6. Temporal evolution of particle distribution during fluidization by lift in a plane Poisuille flow: (a)–(d) contours of particle volume fraction, (e)–(h) gas-phase axial velocity.

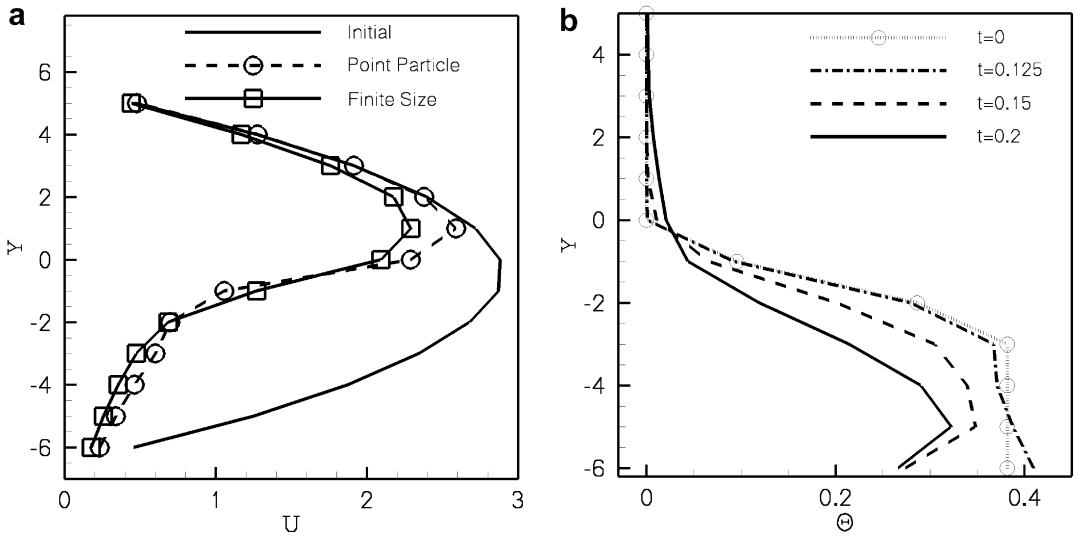

Fig. 7. Vertical variation of mean gas-phase axial velocity and particle volume fractions at different times. The time evolutions are obtained using the finite-size approach. (a) Gas-phase mean axial velocity; (b) particle mean volume fraction.

sponding mean velocities from the point-particle formulation. Both approaches start with parabolic profiles for the fluid velocity. As the particles accelerate from rest, the inter-phase drag force decelerates the fluid flow in the bottom half of the channel as shown by the decreased fluid velocity. This is solely due to the inertia of the particles, and both models predict similar mean velocity profiles at late times. Small deviations in mean axial velocity in the particle region exist between the two formulations. Fig. 7b shows the time evolution of the mean particle volume fraction predicted by the finite-size particles. Initially, the volume fraction is constant in the bottom half of the channel, since the particles are at rest. As the particles accelerate, the near-wall volume fraction decreases, and the volume fraction in the center of the channel increases. In other words, the closely packed particles near the wall push the array of particles upward.

Fig. 8 shows the vertical variation of the rms axial and vertical velocities at different times in the simulation. With increasing time, the rms fluctuations in the axial and vertical velocities increase. The locations of high fluctuations correspond to large gradients in the volume fraction (see Fig. 7b). It should be noted that the rms velocity fluctuations obtained using the point-particle approach were negligible, and did not change with time.

As mentioned earlier, the finite-size formulation can alter the flow evolution through the inter-phase momentum exchange and the modification of the continuity and momentum equations. The velocity field is no longer divergence-free in the region of variations in particle volume fractions: $\frac{1}{\Theta_f}\frac{D\Theta_f}{Dt} = -\nabla\cdot(\mathbf{u}_f)$. This has a direct effect on the Poisson equation (23), altering the pressure field through a local source term. On the other hand, the commonly used point-particle implementation neglects

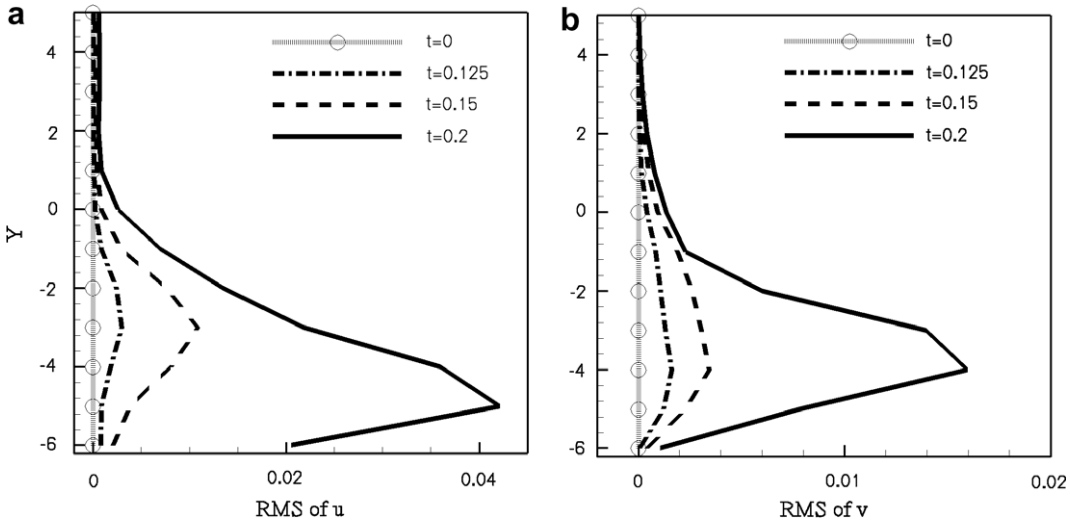

Fig. 8. Vertical variation of rms velocity at different times using the finite-size approach: (a) rms of axial velocity, u'; (b) rms of vertical velocity, v'.

any variations in volume fraction by setting $\frac{D\Theta_f}{Dt} = 0$. The point-particle assumption does not necessarily imply $\frac{D\Theta_f}{Dt} = 0$, however, it is implicitly assumed in most large-eddy and direct numerical simulations of particle-laden flows. In order to numerically evaluate the effect of the continuity equation in the finite-size approach, we artificially imposed divergence-free constraint (by setting $\delta\rho/\delta t = 0$) in the Poisson equation. The results obtained were very similar to the point-particle approach, and did not produce any lift of the particles.

These results indicate that the blocking effect of particles on the fluid phase, modeled by the continuity equation in the finite-size approach alters the fluid flow in regions of high gradients in volume fraction. Several tests with higher grid resolution, varied density ratios were performed to obtain similar results. It should be noted that, the mechanism of lift observed in the fully resolved DNS simulations (Choi and Joesph, 2001) is different from the one given by finite-size model. In the model, we *do not* consider rotation of the particles, whereas the DNS includes particle rotation altering the flowfield immediately surrounding the particle. The effect of particle rotation and the corresponding lift produced can be modeled in the finite-size approach by solving for the angular velocity of the particles and modeling the torque exerted on them through correlations similar to the drag laws. This may change the velocity and the evolution of particles which will alter the volume fraction fields. However, it is shown that even without these rotational effects, the finite-size formulation predicts the particle evolution in qualitative agreement with the fully resolved DNS (Choi and Joesph, 2001).

5. Summary and conclusions

In the present work, we compared the point-particle and finite-size formulations for three different rigid particulate flows. Our objective is to investigate the effect of particle volume fractions on the flow development. For the first case of gravitational settling, the particle evolution obtained from point-particles and the finite-size model are similar. This is mainly because, the flow is gravity- and collision-dominated. For the case of jet-fluidization, however, the particle evolutions predicted by the two approaches are completely different. The patterns observed in Fig. 2a are absent when simulated using point-particles (Fig. 2b). Also, for the particle-laden Poisuille flow, point-particles do not predict any lift and fluidization. This indicates that inter-phase momentum exchange modeled as point-sources in two-way coupling of the point-particle approach is not sufficient to produce the effects observed in fully resolved direct numerical simulations of these flows.

These findings suggest that LES/DNS of two-phase turbulent flows should take into account the fluid volume displaced by the particles. Even for dilute loadings, the preferential concentration of heavy particles observed in many turbulent flows will result in local clustering of particles. Even small variations in fluid volume fractions can alter the local pressure by producing a non-divergence-free velocity field. These effects will become more important in wall-bounded flows. As pointed by Segura et al. (2004), the typical LES or DNS studies of particle-laden channel flows involve grid resolutions that are finer than the particle size in the wall-normal direction. Under such conditions, the point-particle assumption is invalid. In addition, the particles near the wall tend to move slowly and have increased residence times. This may result in increased variations in fluid volume fractions and the effect of the finite-size of the particles near the channel walls can comparable to the inter-particle and particle–wall collisions (Prosperetti and Zhang, 1995). Our present study indicates that the finite-size approach can capture the local flow blocking effects and alters the fluid flow. These effects may become important to predict accurate trends of particle–turbulence interactions.

Note that the finite-size formulation can be applied to large-eddy simulations by applying a density-weighted Favre-filtering operations to the governing equations similar to variable density, turbulent reacting flows. Furthermore, applications involving dense flows such as liquid-fuel atomization in automotive and aircraft engines, should account for the finite-size of the droplets/particles in order to predict the evolution of the fuel mass fractions correctly. As demonstrated in this work, Kelvin–Helmholtz type instability waves created by denser fuel flowing into a lighter fluid can be captured by this model. This may allow better representation of the important features of primary atomization, often neglected in these types of simulations (Moin and Apte, 2006).

Acknowledgments

This work was supported by the Department of Energy's Advanced Scientific Computing Program. SVA also acknowledges support from Office of Naval Research under the grant number N000140610697 supervised by Dr. Ki-Han Kim. A major part of this work was performed when SVA was in residence at Stanford University.

References

Andrews, M.J., O'Rourke, P., 1996. The multiphase particle-in-cell (MP-PIC) method for dense particle flow. Int. J. Multiphase Flow 22, 379–402.

Apte, S.V., Mahesh, K., Moin, P., Oefelein, J.C., 2003a. Large-eddy simulation of swirling particle-laden flows in a coaxial-jet combustor. Int. J. Multiphase Flow 29, 1311–1331.

Apte, S.V., Gorokhovski, M., Moin, P., 2003b. LES of atomizing spray with stochastic modeling of secondary breakup. Int. J. Multiphase Flow 29, 1503–1522.

Apte, S.V., Mahesh, K., Ham, F., Iaccarino, G., Constantinescu, G., Moin, P., 2004. Large-eddy simulation of multiphase flow in complex combustors. In: Mammoli, A.A., Brebbia, C.A. (Eds.), In: Computational Methods in Multiphase Flow, vol. 2. WIT Press, UK, pp. 53–62.

Bagchi, P., Balachandar, S., 2003. Effect of turbulence on the drag and lift of a particle. Phys. Fluids 15, 3496–3513.

Burton, T.M., Eaton, J.K., 2003. Fully resolved simulations of particle–turbulence interaction. Report No. TSD-151, Department of Mechancial Engineering, Stanford University.

Choi, H.G., Joesph, D.D., 2001. Fluidization by lift of 300 circular particles in plane Poisuille flow by direct numerical simulation. J. Fluid Mech. 438, 101–128.

Crowe, C., Sommerfeld, M., Tsuji, Y., 1998. Multiphase Flows with Droplets and Particles. CRC Press.

Cundall, P.A., Strack, O.D.L., 1979. A discrete numerical model for granular assemblies. Geotechnique 29, 47–65.

Ding, J., Gidaspow, D., 1990. A bubbling fluidization model using kinetic theory of granular flow. AIChE 36, 523–537.

Dukowicz, J.K., 1980. A particle–fluid numerical model for liquid sprays. J. Comput. Phys. 35, 229–253.

Eldredge, J.D., Colonius, T., Leonard, A., 2002. A vortex-particle method for two-dimensional compressible flow. J. Comput. Phys. 179, 371–399.

Elghobashi, S., 1984. On predicting particle-laden turbulent flows. Appl. Sci. Res. 52, 309–329.

Ferrante, A., Elghobashi, S., 2004. On the physical mechanisms of drag reduction in a spatially-developing turbulent boundary layer laden with microbubbles. J. Fluid Mech. 503, 345–355.

Gidaspow, D., 1994. Multiphase Flow and Fluidization Continuum and Kinetic Descriptions. Academic Press, Boston, MA.

Joseph, D.D., Lundgren, T., 1990. Ensemble averaged and mixture theory equations for incompressible fluid–particle suspensions. Int. J. Multiphase Flow 16, 35–42.

Kajishima, T., Takiguchi, S., 2002. Interaction between particle clusters and particle-induced turbulence. J. Heat Fluid Flow 23, 639–646.

Mahesh, K., Constantinescu, G., Moin, P., 2004. A new time-accurate finite-volume fractional-step algorithm for prediction of turbulent flows on unstructured hybrid meshes. J. Comput. Phys. 197, 215–240.

Maxey, M.R., Patel, B.K., 2001a. Localized force representations for particles sedimenting in Stokes flow. Int. J. Multiphase Flow 27, 1603–1626.

Moin, P., Apte, S.V., 2006. Large-eddy simulation of multiphase flow in complex combustors. AIAA J. 44, 698–710.

Patankar, N.A., Joseph, D.D., 2001a. Modeling and numerical simulation of particulate flows by the Eulerian–Lagrangian approach. Int. J. Multiphase Flow 27, 1659–1684.

Patankar, N.A., Joseph, D.D., 2001b. Lagrangian numerical simulation of particulate flows. Int. J. Multiphase Flow 27, 1685–1706.

Prosperetti, A., Zhang, D.Z., 1995. Finite-size effects in disperse two-phase flows. Theor. Comput. Fluid Dyn. 7, 429–440.

Reade, W.C., Collins, L.R., 2000. Effect of preferential concentration on turbulent collision rates. Phys. Fluids 12, 2530–2540.

Rouson, D.W.I., Eaton, J.K., 2001. On the preferential concentration of solid particles in turbulent channel flow. J. Fluid Mech. 348, 149–169.

Segura, J.C., Eaton, J.K., Oefelein, J.C., 2004. Predictive capabilities of particle-laden LES. Report No. TSD-156, Department of Mechanical Engineering, Stanford University.

Snider, D.M., 2001. An incompressible three-dimensional multiphase particle-in-cell model for dense particulate flows. J. Comput. Phys. 170, 523–549.

Sommerfeld, M., Ando, A., Qiu, H.H., 1992. Swirling, particle-laden flows through a pipe expansion. J. Fluids Eng. 114, 648–656.

Wang, Q., Squires, K.D., 1996. Large eddy simulation of particle-laden turbulent channel flow. Phys. Fluids 8, 1207–1223.

Xu, J., Maxey, M., Karniadakis, G., 2002. Numerical simulation of turbulent drag reduction using micro-bubbles. J. Fluid Mech. 468, 271–281.